Optimizing the 1B-adrenergic receptor for solution NMR studies

Schuster, Matthias ; Deluigi, Mattia ; Pantić, Milica ; Vacca, Santiago ; Baumann, Christian ; Scott, Daniel J ; Plückthun, Andreas ; Zerbe, Oliver

Abstract: Sample preparation for NMR studies of G protein-coupled receptors faces special requirements: Proteins need to be stable for prolonged measurements at elevated temperatures, they should ideally be uniformly labeled with the stable isotopes 13C, 15N, and all carbon-bound protons should be replaced by deuterons. In addition, certain NMR experiments require protonated methyl groups in the presence of a perdeuterated background. All these requirements are most easily satisfied when using Escherichia coli as the expression host. Here we describe a workflow, starting from a temperature-stabilized mutant of the 1B-adrenergic receptor, obtained using the CHESS methodology, into an even more stable species, in which flexible parts from termini were removed and the intracellular loop 3 (ICL3) was stabilized against proteolytic cleavage. The yield after purification corresponds to 1–2 mg/L of D2O culture. The final purification step is ligand-affinity chromatography to ensure that only well-folded ligand-binding protein is isolated. Proper selection of detergent has a remarkable influence on the quality of NMR spectra. All optimization steps of sequence and detergent are monitored on a small scale by monitoring the melting temperature and long-term thermal stability to allow for screening of many conditions. The stabilized mutant of the 1B-adrenergic receptor was additionally incorporated in nanodiscs, but displayed slightly inferior spectra compared to a sample in detergent micelles. Finally, both [15N,1H]- as well as [13C,1H]-HSQC spectra are shown highlighting the high quality of the final NMR sample. Importantly, the quality of [13C,1H]-HSQC spectra indicates that the so prepared receptor could be used for studying side-chain dynamics.

DOI: https://doi.org/10.1016/j.bbamem.2020.183354

BBA - Biomembranes 1862 (2020) 183354

Contents lists available at ScienceDirect

BBA - Biomembranes

journal homepage: www.elsevier.com/locate/bbamem

Optimizing the α_{1B}-adrenergic receptor for solution NMR studies

Matthias Schuster[a], Mattia Deluigi[b], Milica Pantić[a], Santiago Vacca[b], Christian Baumann[a], Daniel J. Scott[c], Andreas Plückthun[b], Oliver Zerbe[a,*]

[a] Department of Chemistry, University of Zurich, Winterthurerstrasse 190, 8057 Zurich, Switzerland
[b] Department of Biochemistry, University of Zurich, Winterthurerstrasse 190, 8057 Zurich, Switzerland
[c] Florey Institute of Neuroscience and Mental Health, Department of Biochemistry and Molecular Biology, The University of Melbourne, 30 Royal Parade Parkville, 3052, Victoria, Australia

ARTICLE INFO

Keywords:
G protein-coupled receptor
Detergent
Helical membrane protein
Solution NMR
Adrenergic receptors

ABSTRACT

Sample preparation for NMR studies of G protein-coupled receptors faces special requirements: Proteins need to be stable for prolonged measurements at elevated temperatures, they should ideally be uniformly labeled with the stable isotopes ^{13}C, ^{15}N, and all carbon-bound protons should be replaced by deuterons. In addition, certain NMR experiments require protonated methyl groups in the presence of a perdeuterated background. All these requirements are most easily satisfied when using *Escherichia coli* as the expression host. Here we describe a workflow, starting from a temperature-stabilized mutant of the α_{1B}-adrenergic receptor, obtained using the CHESS methodology, into an even more stable species, in which flexible parts from termini were removed and the intracellular loop 3 (ICL3) was stabilized against proteolytic cleavage. The yield after purification corresponds to 1–2 mg/L of D_2O culture. The final purification step is ligand-affinity chromatography to ensure that only well-folded ligand-binding protein is isolated. Proper selection of detergent has a remarkable influence on the quality of NMR spectra. All optimization steps of sequence and detergent are monitored on a small scale by monitoring the melting temperature and long-term thermal stability to allow for screening of many conditions. The stabilized mutant of the α_{1B}-adrenergic receptor was additionally incorporated in nanodiscs, but displayed slightly inferior spectra compared to a sample in detergent micelles. Finally, both [^{15}N,^{1}H]- as well as [^{13}C,^{1}H]-HSQC spectra are shown highlighting the high quality of the final NMR sample. Importantly, the quality of [^{13}C,^{1}H]-HSQC spectra indicates that the so prepared receptor could be used for studying side-chain dynamics.

1. Introduction

G protein-coupled receptors (GPCRs) are 7-helix integral membrane proteins of high pharmacological interest [1]. There are over 800 human GPCRs recognizing a myriad of different ligands and playing a crucial role in a plethora of cellular processes. Through conformational changes, GPCRs transduce extracellular stimuli across the membrane to intracellular effectors such as heterotrimeric G proteins and β-arrestins. X-ray crystallography has provided structures of GPCRs in ligand-free apo states, in antagonist- and agonist-bound states, bound to G proteins and mimics thereof as well as to β-arrestins. This knowledge, which has been further expanded in recent years by cryo-EM structures of GPCRs in complex with intracellular effectors, has tremendously enhanced our understanding of how these receptors function [2,3].

GPCRs sample different conformational states (inactive, intermediate, active), and ligands act on GPCRs by modulating the equilibrium between these states [4]. Sampling of active states in the ligand-free form results in receptor basal activity, while agonist binding serves to shift the equilibrium towards active states [5,6]. Conformational changes in conserved regions, called micro-switches, dictate the large-scale helical rearrangements associated with receptor activation and biased signaling [7,8]. To fully comprehend the mode of action of these micro-switches, the different states of the receptor must be understood in molecular detail, including populations, transitions and interconversion rates of different conformations, as well as a further delineation of conformational sub-states. Such a comprehensive picture of receptor dynamics is difficult to obtain exclusively from crystallography, because the structures represent only snapshots of particular conformations, and conformations separated by small energy gaps can be influenced by crystal packing forces. In addition, successfully crystallized GPCRs are often modified by insertion of proteins, such as lysozyme, into flexible loops to provide crystal contacts and usually require high-affinity inverse agonists to be bound to further rigidify the structure.

* Corresponding author at: Department of Chemistry, University of Zurich, Winterthurerstrasse 190, CH-8057 Zurich, Switzerland.
E-mail address: oliver.zerbe@chem.uzh.ch (O. Zerbe).

https://doi.org/10.1016/j.bbamem.2020.183354
Received 13 March 2020; Received in revised form 1 May 2020; Accepted 9 May 2020
Available online 13 May 2020

In principle, solution NMR spectroscopy is capable of quantifying receptor dynamics at the level of side chain rearrangements using various flavors of relaxation measurements [9]. Unfortunately, the instability of native receptors precludes measurements at the elevated temperatures required to obtain NMR spectra of sufficient quality, impeding resonance assignment and determination of relaxation rates. In addition, native receptors typically display very low expression levels, making it challenging to isolate the milligram amounts of pure and homogeneous protein required for NMR studies. An important first step in any GPCR solution-state NMR study is therefore the optimization of the protein construct to improve expression levels in minimal medium and to increase thermal stability. To overcome the protein instability problem, many receptors have been stabilized by introducing point mutations using alanine scanning mutagenesis or directed evolution, or through complexation with binders such as nanobodies [10,11].

GPCRs used in crystallographic studies have mostly been produced in insect cells, but also in mammalian cells, yeast, or *E. coli*. To assign proteins of the size of a GPCR using traditional triple-resonance NMR experiments, uniform ^{2}H, ^{13}C, ^{15}N labeling is required. *E. coli* is therefore the preferred host as it allows for culturing in heavy water, in contrast to insect cells. Alternatively, spectra can be assigned from point mutants, but this can be laborious, and mutations can often result in larger changes in the spectra, resulting in ambiguous assignments, or the point mutants may even alter properties of the protein.

Our work relied on directed evolution to generate thermostabilized GPCR mutants that can be produced in *E. coli* and are stable at elevated temperatures in detergent micelles. Briefly, mutants were generated by the CHESS method [12], in which *E. coli* cells expressing a library of mutants are encapsulated to retain the genotype-phenotype linkage after solubilization in detergent, followed by selection of stable variants via binding of a fluorescently-labeled ligand [12].

In this study we describe the production of an NMR sample of a thermostabilized human α_{1B}-adrenoceptor (α_{1B}-AR). During this study, the thermal stability of the receptor was further improved and flexible regions were truncated, resulting in a monomeric receptor construct that expressed sufficiently well to allow preparation of an NMR sample (220 µL of 450 µM receptor) from 3 L of culture. Importantly, the GPCR was stable at 47 °C for weeks in detergent micelles and in phospholipid nanodiscs. We show how biophysical and chromatographic techniques were used to guide the optimization process and present ^{15}N- and ^{13}C-HSQC spectra of the perdeuterated receptor.

2. Results

2.1. Selection of stabilized mutants and construct optimization

The α_{1B}-AR mutant #12, previously obtained by CHESS stabilization, was used as the starting variant [13]. This receptor mutant contained 8 amino acid mutations compared to the native human sequence (Table S1). Some of the initial biophysical characterization described below was performed on this mutant. Subsequently, N- and C-terminal truncations as well as an intracellular loop 3 deletion were implemented to avoid degradation by *E. coli* proteases thereby reducing the number of mutations to 6. Preliminary tests of this receptor mutant solubilized in dodecyl maltoside (DDM) revealed insufficient stability at temperatures desired for measuring triple-resonance NMR spectra for backbone assignment. Therefore, an additional round of CHESS stabilization was performed. Details of this procedure will be published elsewhere.

Fig. 1A describes the process that led to the final receptor construct. Following the initial CHESS stabilization, several mutants were tested for thermal stability. The most stable mutant, called B1, harbors 14 mutations (Table S1). Analogously to α_{1B}-AR-#12, N- and C-terminal truncations as well as an intracellular loop (ICL) 3 deletion were implemented, reducing the number of mutations to 13 (Fig. S1).

For expression in *E. coli*, the genes encoding the receptor constructs were cloned into a pBR322-derived vector designed by Grisshammer et al. and modified by Egloff et al. [14,15]. In this vector the receptor is expressed as a fusion with N-terminal maltose-binding protein (MBP) and C-terminal thioredoxin A (TrxA) (Fig. 1B). The N-terminal signal peptide of the MBP moiety results in the secretion of MBP into the periplasm, and therefore directs the fused GPCR into the *E. coli* cytoplasmic membrane in the correct N-out, C-in topology.

The fusion partners were cleaved off during purification by means of 3C protease cleavage sites, and an additional His- or Avi-tag were inserted to allow for additional separations. A schematic representation of the used constructs is shown in Fig. 1B.

2.2. Optimization of expression

The size of the optimized constructs after removal of the fusion proteins was ~34 kDa. Triple-resonance experiments for backbone assignment of proteins of this size require triply-labeled [^{2}H,^{13}C,^{15}N] proteins and hence expression in deuterated M9 minimal media. Optimized expression conditions are therefore crucial for receptors with low expression yields, in particular when considering the high cost for isotopically labeled media.

The expression levels were quantified with a radioligand binding assay (RLBA) using ^{3}H-prazosin as the radioligand. Prazosin is a small-molecule antagonist which selectively binds to α_1-ARs with nanomolar affinity. Here we only show results obtained with the α_{1B}-AR mutant #12, which was used for optimization of the conditions, but the mutant B1 displayed very similar receptors/cell counts (Fig. 2). The highest expression levels were observed at 30 °C. Expression was quite slow, and only after 14 h of expression was the maximum number of receptors/cell observed at 30 °C in light water, which then only slightly decreased over the next 48 h (data not shown). Interestingly, expression levels in minimal M9 medium were significantly higher than in the rich LB or TB media (~20,000 receptors/cell in M9 compared to ~10,000 receptors/cell in LB). However, the final cell mass is typically significantly lower in M9 compared to rich media. Further experiments revealed the limiting effect of glucose and NH_4Cl concentrations on the final optical density at 600 nm (OD_{600}) for overnight growth at 30 °C. With increased glucose and NH_4Cl concentrations, cell masses comparable to LB and TB media could be achieved.

The expression in deuterated M9 media was also monitored with a RLBA. To this end cells were grown in M9 media with 1 g/L NH_4Cl and 6 g/L glucose or glycerol. Surprisingly, expression levels were the same in D_2O or H_2O when using glucose as the carbon source and only the final cell density was slightly lower in D_2O. The expression in M9 D_2O could be performed with yields comparable to those in M9 H_2O. In contrast, expression levels dropped dramatically in D_2O when using glycerol as the carbon source. Without induction, the cells grown in the presence of deuterated glycerol reached an even higher OD_{600} than the cells grown in the presence of deuterated glucose (data not shown). Therefore, it seems that expression with glycerol in D_2O is inhibiting cell growth. We suspect that the lac-promoter is more active in the absence of glucose, and the expression rate is too fast to allow proper receptor insertion into the *E. coli* membrane.

According to the RLBA, the amount of functional receptor before purification was estimated as 4.1 mg per L of M9 culture in case of expression in D_2O with 6 g/L glucose.

2.3. Receptor purification

The α_{1B}-AR constructs were purified using a two-column strategy in order to obtain homogeneous and pure receptors. Fig. 3 shows the schematic overview of the two-column strategy.

The cells were lysed with lysozyme and dodecyl maltoside/cholesteryl hemisuccinate (DDM/CHS). Solubilization with DM or DDM alone resulted in a lower yield, while the milder lauryl maltose neopentyl glycol (LMNG) could not effectively solubilize the cells under these

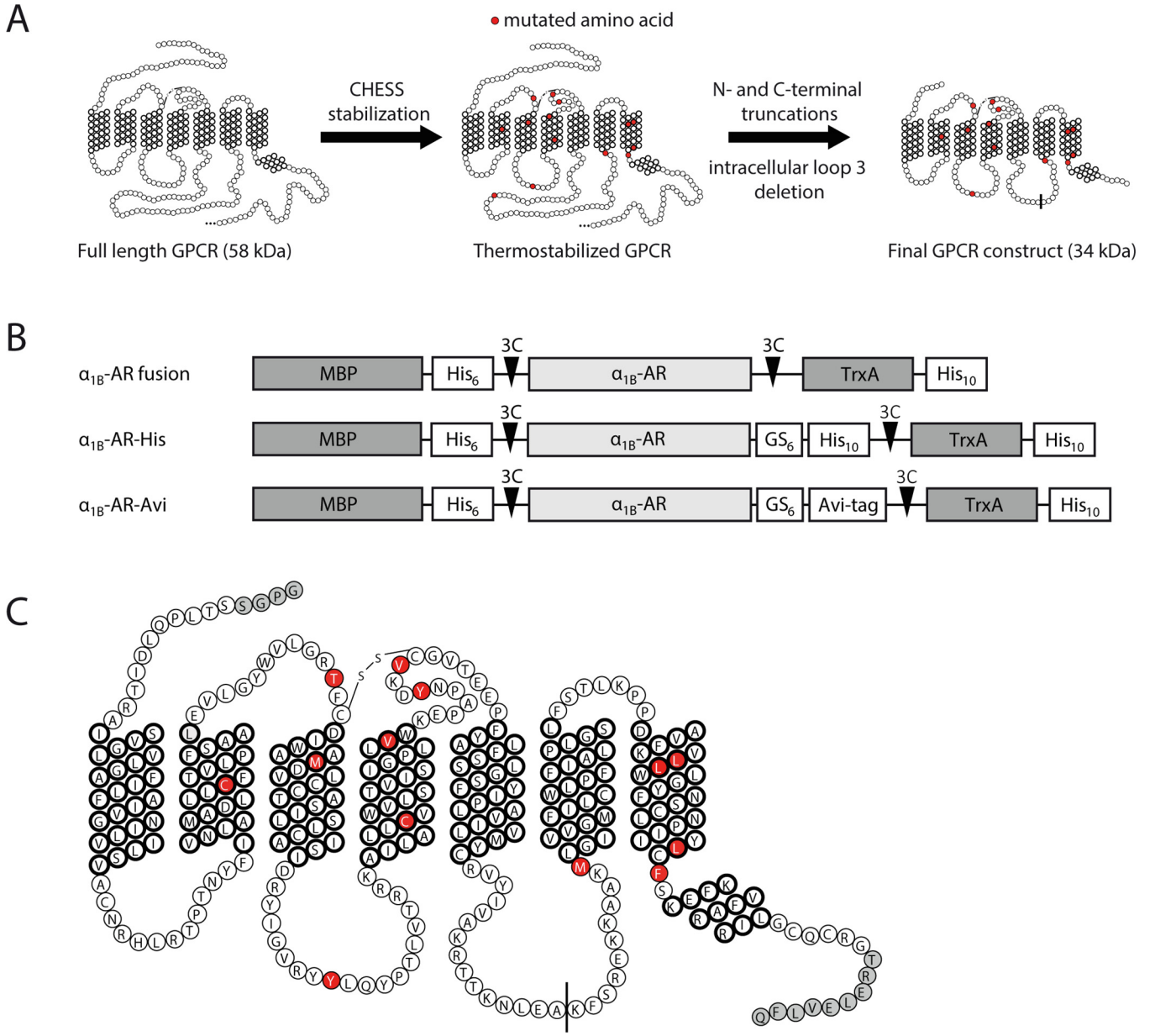

Fig. 1. Design of the stabilized α_{1B}-AR construct. **A** Following CHESS stabilization flexible parts were removed. **B** Expression constructs showing the location of the N-terminal maltose-binding protein (MBP) and the C-terminal thioredoxin A (TrxA) fusions, the affinity tags for purification and the 3C cleavage sites. **C** Snake plot of the α_{1B}-AR-B1D1 construct, harboring the set of B1 mutations and the ICL3 deletion D1 (Table S1, Fig. S1). Additional linker amino acids and the 3C site are shown in grey and the 13 mutations in red (one mutation originally selected in the intracellular loop 3 is not shown here as it is in a region deleted in this final construct). Transmembrane (TM) helices are chosen as predicted by UniProt. (For interpretation of the references to colour in this figure legend, the reader is referred to the web version of this article.)

conditions.

After solubilization, the soluble fraction was incubated with TALON resin. The receptor construct was selectively bound via its His-tags to resin-bound Co^{2+}. We observed purer samples using Co^{2+}-TALON resin compared to Ni^{2+}-NTA. Optimization of the incubation time and the amount of resin was crucial to maximize binding of the receptor. Optimal conditions were obtained when using 1 mL of TALON resin per g of cells and an incubation time of at least 2.5 h.

Detergent was exchanged on the TALON column to LMNG, in which the receptor was more stable for the subsequent overnight 3C cleavage. The receptor was eluted from the TALON column with EDTA instead of imidazole because imidazole proved to be a low-affinity ligand of the α_{1B}-AR and inhibited binding to the prazosin ligand column.

The second purification step was performed with a prazosin ligand column (prepared in-house, manuscript in preparation). A cleavable prazosin derivative was covalently coupled via a protein scaffold to Sepharose beads in a similar way as described by Egloff et al. [16]. Binding to the column was carried out overnight, simultaneously with the 3C cleavage. The ligand column possibly exhibits a K_d value similar to the fluorescently-labeled prazosin derivative BODIPY-FL-prazosin, also called QAPB (8.5 nM to α_{1B}-AR-#12), as it is modified at the same site [13]. The receptor can be eluted from the column by competition with a low-affinity ligand such as imidazole or with a high-affinity ligand like prazosin. The latter cannot be removed afterwards, whereas imidazole can be efficiently removed by desalting and dialysis, allowing the purification of receptor samples in the apo-state. Removal of the fusion proteins, 3C protease and the aggregated receptors with this ligand column resulted in very pure and homogeneous receptor samples.

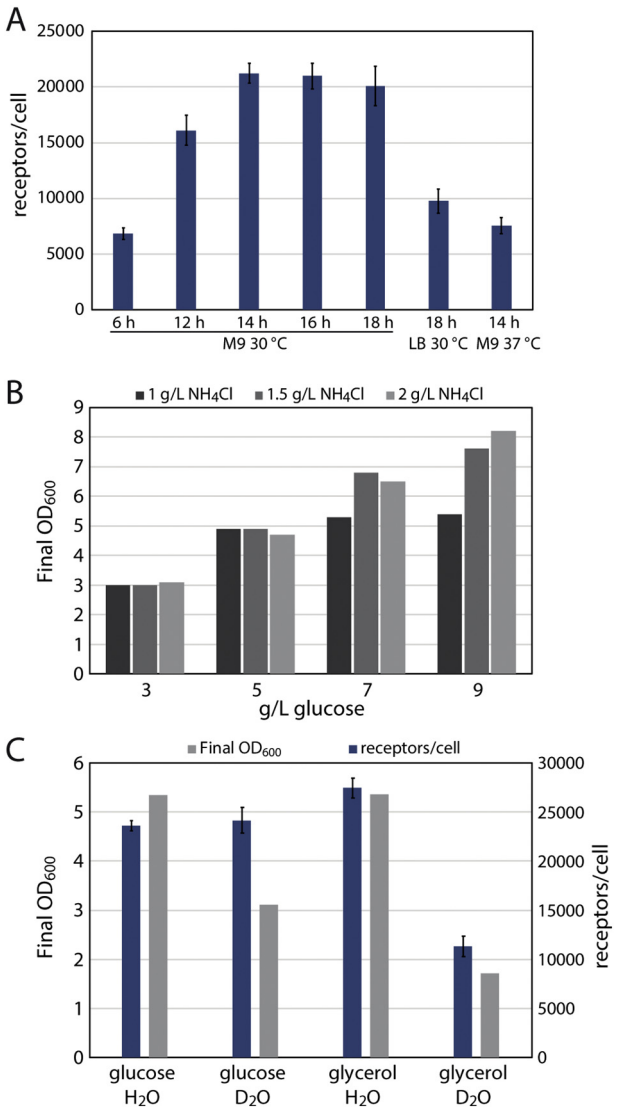

Fig. 2. Optimization of growth and expression conditions. **A** Receptors per cell count from RLBAs when varying temperature and medium composition. Error bars indicate the standard deviation of triplicates. **B** Final OD_{600} after overnight growth of BL21 cells at 30 °C with varying amounts of glucose and NH_4Cl. **C** Comparison of final OD_{600} and receptors/cell after expression in light and heavy water using different carbon sources.

The final yield after purification strongly depended on the mutant, the details of expression and the detergent used. In general, up to 50% of the receptor estimated by RLBA on cells could be recovered after purification, which resulted in a yield of up to 2 mg per L of M9 expression culture in D_2O with 6 g/L glucose.

2.4. Loop deletions and truncations of the α_{1B}-AR mutants

We observed degradation in the ICL3 on the SDS-PAGE gel (Fig. S2), likely by *E. coli* proteases, and hence we tested deletions within the ICL3. The loop deletions were already tested with the α_{1B}-AR-#12 mutant and were further transferred to the α_{1B}-AR-B1 mutant, which was obtained by a second CHESS round from the #12 mutant. Loop deletion variants are characterized by an additional letter D in their name from now on, and they are described in Fig. S1.

We monitored stabilizing effects of various ICL3 deletions, as well as an additional reduction in size. To test thermostability under conditions more closely resembling those used in the NMR experiments (high receptor concentrations and high temperatures), the stability was measured with a SEC-based assay. To this end, the receptor was incubated at concentrations between 50 and 100 μM for multiple days at a chosen temperature. The stability of the receptor could be deduced from the change in intensity of the monomeric peak in the SEC chromatogram.

Loop deletions D2 and D7 (Fig. S1) showed a significant reduction in stability at 47 °C, while D1, D4 and D5 were comparably stable (Fig. S3). To obtain a more homogeneous sample for NMR studies, the receptor mutant B1 with the ICL3 deletion D1, called α_{1B}-AR-B1D1, was chosen as the final construct. This α_{1B}-AR construct starts at S35 and ends at G369 after helix 8, it includes deletion of ICL3 residues G240–F284 and contains 4 additional N-terminal and 9 C-terminal amino acids used as linker or belonging to the cleaved 3C cleavage site (Fig. 1C).

2.5. Characterization of the receptor constructs

The α_{1B}-AR constructs were characterized with different methods to confirm that the purified receptor samples were pure and monomeric. The test for ligand-binding capability was already incorporated into the purification procedure, as the receptor was captured onto a ligand column and it was eluted by competitive ligand binding.

Reproducible purity was achieved for similar constructs in different detergents. Samples were usually fairly pure after TALON purification, and highly pure (> 95%) after the prazosin column (Fig. 4A). The high purity and the correct receptor mass were further confirmed via ESI-MS. Higher cone energies helped to remove bound LMNG moieties with additional masses of 1005 Da (Fig. 4B).

The stability of the receptor mutant was also analyzed with a 7-diethylamino-3-(4′-maleimidylphenyl)-4-methylcoumarin (CPM) assay [17]. Therein, thermal unfolding is monitored by the increase in fluorescence of the CPM dye upon binding to cysteines and hydrophobic patches exposed during protein denaturation [18]. Fig. 4D shows that the α_{1B}-AR-B1 receptor construct has an apparent T_m of 76 °C in DDM/CHS, indicating an exceptionally high stability compared to other GPCRs measured under similar conditions [19].

The K_d values for the wild-type (wt) α_{1B}-AR receptor as well as for the B1 and #12 mutants were determined using a RLBA. We determined a value of 0.07 nM for the wt receptor, 0.80 nM for the B1 mutant and 1.18 nM for the #12 mutant (Fig. 4C). The affinity of prazosin for the mutant α_{1B}-AR proteins is thus still very strong.

The homogeneity of the α_{1B}-AR constructs was also analyzed by SEC on a Superdex 200 column (Fig. 5). After the ligand-affinity column purification the receptor showed a very homogeneous peak. We applied multi-angle-light-scattering (MALS) coupled to SEC to determine the absolute mass of the receptor in detergent micelles. Two detectors, capable of determining the concentration (UV and refractive index, RI), allow to deconvolute the total mass into the masses of the protein and of the detergent micelle. Thereby, MALS allows determination of the oligomeric state of the protein in the detergent micelles. For the detergents, the dn/dc values were determined with a calibration curve. For DDM/CHS, a value of 0.1569 ± 0.0035 mL/g was measured, close to the published value [20], while for LMNG a value of 0.1382 ± 0.0010 mL/g was determined. Together with the standard dn/dc value for proteins of 0.185 mL/g, the composition of the protein/micelle complex can be determined.

An accurate measurement was performed with the α_{1B}-AR-#12D2 construct in DDM/CHS (10:1 w/w) and in LMNG (Fig. 5). For the receptor in DDM/CHS a calculated protein mass of 31.5 kDa fits well to the expected molecular weight of 34.4 kDa, clearly revealing that the receptor was monomeric in the micelle. The empty DDM/CHS micelle had a mass of 84 kDa, while in complex with the protein the mass of the detergent was 123.2 kDa, leading to a total protein-detergent mass of 154.7 kDa. In case of the receptor in LMNG detergent, the empty micelle had a calculated mass of 87.8 kDa, while with the receptor the detergent micelle had a mass of 101.2 kDa, and the whole detergent-

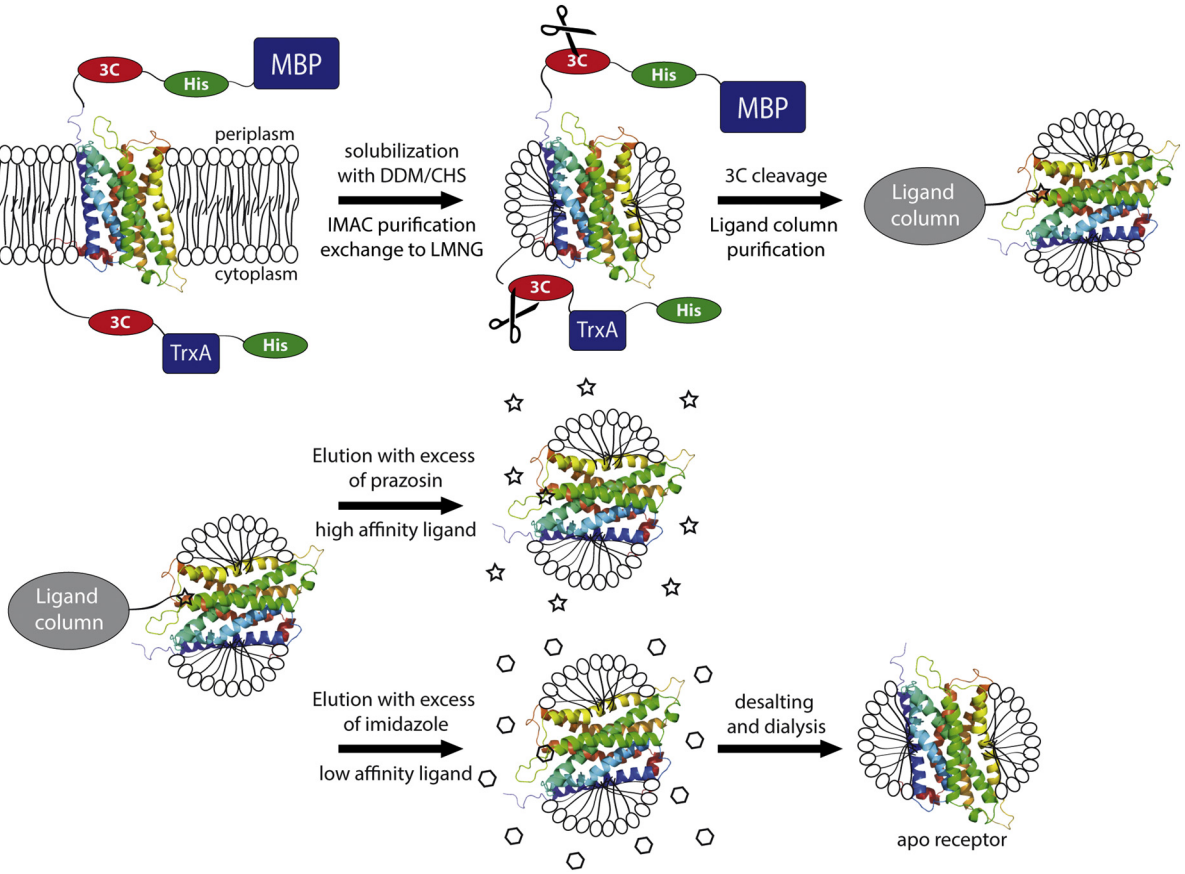

Fig. 3. Schematic overview of the purification strategy. **A** The receptor is extracted from the *E. coli* membrane and solubilized in DDM/CHS micelles. Subsequently, immobilized metal ion affinity chromatography (IMAC) is used to separate the receptor construct from contaminants, after which the fusion proteins are removed. A final purification step involves binding to a ligand column (prazosin column). **B** The receptor can be either eluted with molar excess of a high-affinity ligand like prazosin or with a high concentration of a low-affinity ligand like imidazole, which can subsequently be removed by dialysis to obtain apo-state receptor.

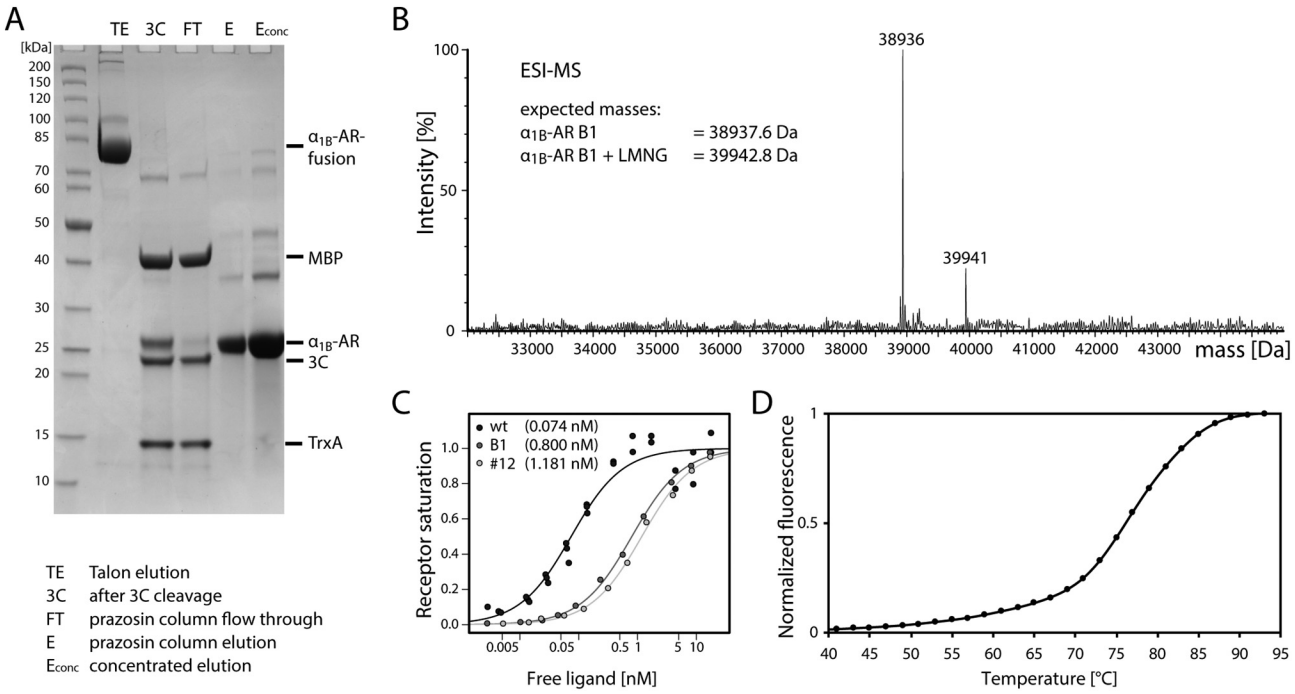

Fig. 4. Characterization of the α_{1B}-AR-B1D1 mutant. **A** SDS-PAGE gel of the α_{1B}-AR-B1D1 mutant purified in LMNG. **B** ESI-MS of the α_{1B}-AR-B1 mutant. **C** K_d values of prazosin for the wild-type (wt) α_{1B}-AR, the B1 and #12 mutants. **D** CPM assay of the α_{1B}-AR-B1 mutant in DDM/CHS with prazosin bound.

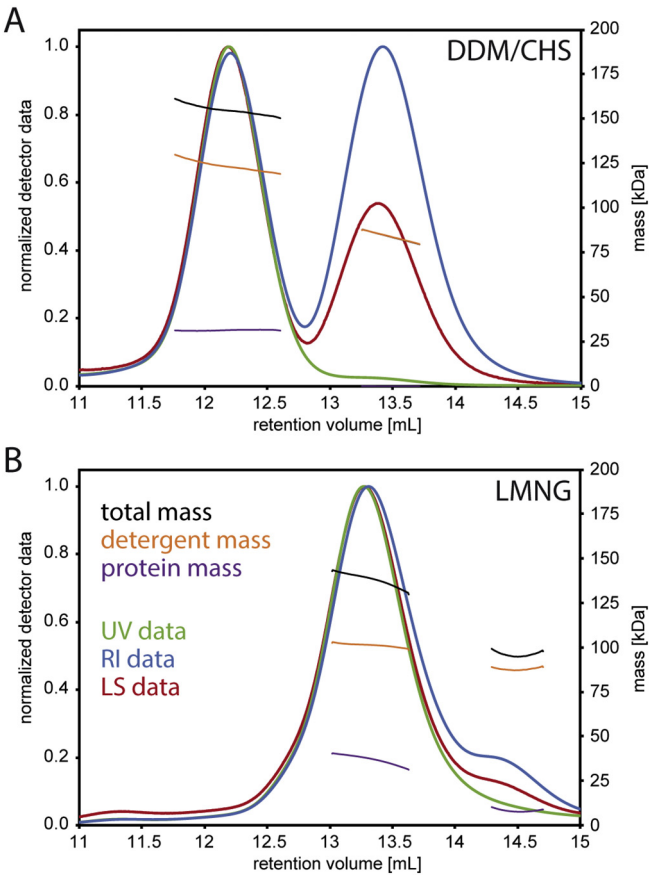

Fig. 5. SEC-MALS diagram of α_{1B}-AR-#12D2. **A** Data in DDM/CHS. **B** Data in LMNG. Depicted are the UV, RI and LS detector data (in green, blue and red, respectively). The lines in black, orange and purple indicate the mass of the complex, the detergent and the protein, respectively. (For interpretation of the references to colour in this figure legend, the reader is referred to the web version of this article.)

protein complex was 138.1 kDa. The protein mass was determined as 36.9 kDa, again in agreement with the expected mass of a monomer. Interestingly, even if the difference in mass between the LMNG and DDM/CHS samples is not very large for both the empty micelles and the protein-detergent complexes, the longer elution times on the gel filtration column indicate that the hydrodynamic radius of the LMNG micelles is smaller.

2.6. Optimizing the choice of detergent

The choice of the optimal detergent is often the most crucial step for successful NMR experiments. Typically, during purification and for functional assays, stabilizing detergents forming large micelles like DDM/CHS are preferred. For solution NMR, however, the size of the protein-detergent complex matters, as a smaller size leads to longer T2 relaxation times and thus sharper peaks. Conversely, smaller detergents may intercalate in the membrane protein and thus help unfold it.

An initial screen to test multiple detergents in parallel was performed with a fluorescence-based assay with biotinylated receptor and streptavidin-coated magnetic beads. The α_{1B}-AR-#12-Avi construct, biotinylated at its C-terminus, was solubilized in DM, immobilized on magnetic beads and saturated with BODIPY-FL-prazosin. The receptor, bound to the magnetic beads, was then exposed to buffers containing different detergents at 4 °C. After incubation in the presence of BODIPY-FL-prazosin for 1 h at 37 °C or 24 h at 37 °C, the beads were washed and the remaining fluorescence signal was measured, corresponding to ligand molecules bound to functional receptor molecules (Fig. 6A).

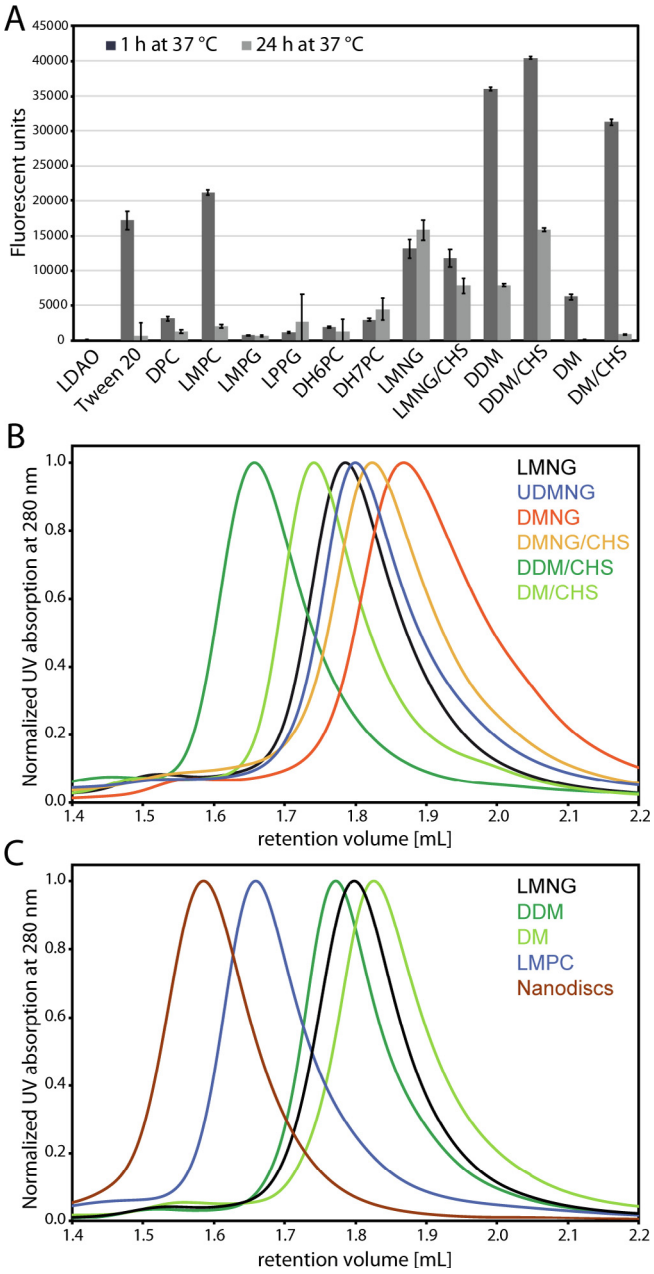

Fig. 6. Stability and size of α_{1B}-AR mutants in different detergents. **A** Measured fluorescence of BODIPY-FL-prazosin bound to the α_{1B}-AR-#12-Avi construct in different detergents after 1 h of incubation at 37 °C (dark grey bars) and after 24 h of incubation at 37 °C (light grey bars). Error bars indicate the standard deviation of the measured triplicates. **B** SEC profiles of α_{1B}-AR-B1 (carrying no ICL3 deletion) in different detergents. **C** SEC profiles of α_{1B}-AR-B1D1-His in different detergents and lipid nanodiscs.

Many detergents already caused precipitation after incubation for 1 h at 37 °C (e.g. in DPC, DH_7PC or LDAO). The highest remaining fluorescence was obtained in DDM and DDM/CHS. A stabilizing effect of CHS was clearly detected when comparing DM/CHS to DM. Measurements after 24 h revealed that a number of other detergents such as LMPC, Tween-20 and DM/CHS did not provide sufficient long-term stability at 37 °C. In general, the maltosides provided the highest stability. The best results were obtained when using LMNG and LMNG/CHS, for which ligand binding was retained even after 24 h at 37 °C. The lower absolute fluorescence levels compared to DDM and DDM/CHS were possibly due to the higher background fluorescence observed in LMNG. It appears, therefore, that LMNG is a well-suited detergent to

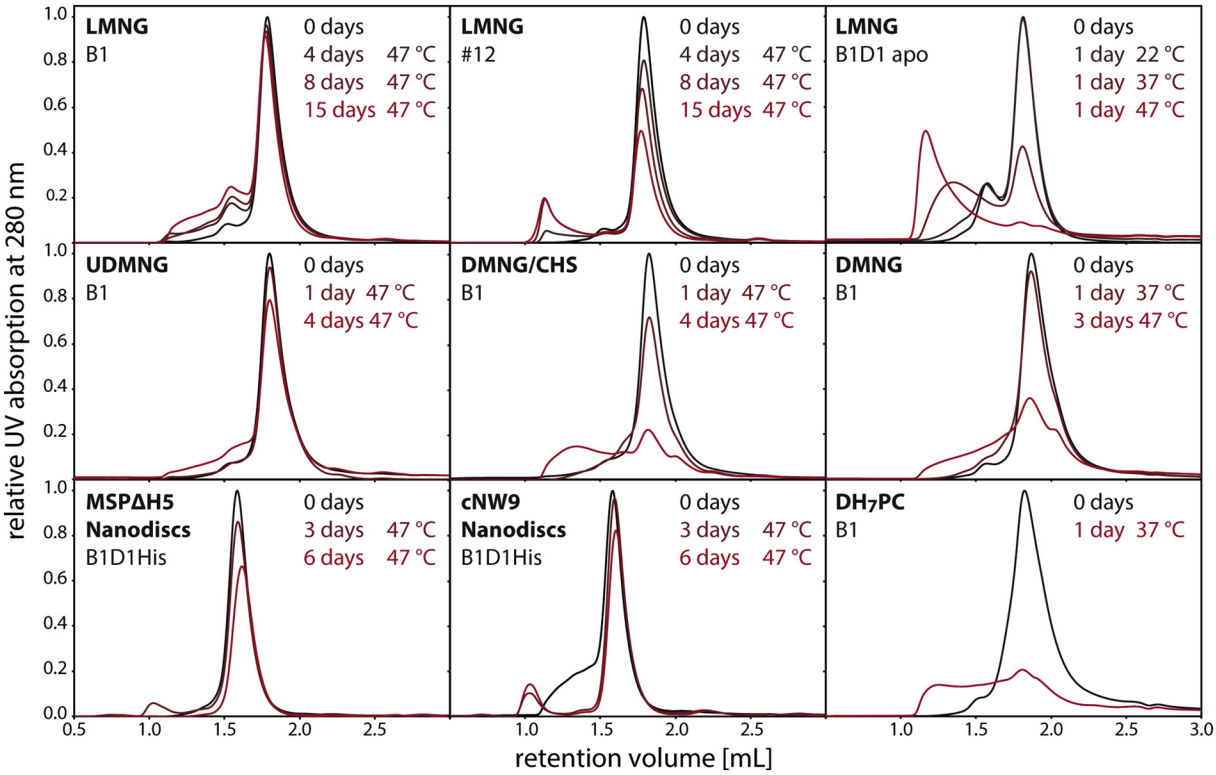

Fig. 7. SEC profiles of α_{1B}-AR receptor mutants in different membrane mimetics. The receptor was always incubated in the presence of prazosin if not mentioned otherwise. Depicted are data before and after incubation at different timepoints and temperatures.

stabilize the receptor for a sufficiently long period of time at high temperatures.

The effect of changes in pH (screened between 6.5 and 8.0) and salt concentration (10 mM – 600 mM), tested in a similar assay with the receptor solubilized in DM at 4 °C, revealed no differences in receptor stability under the different buffer compositions (Fig. S4).

To find out which detergents were most suitable for NMR experiments, a variety of detergents were evaluated with regards to the size of the protein-detergent complex (using SEC), yields of purified protein and long-term thermostability (Fig. 7). To this end, the B1D1 receptor construct was solubilized and purified in DDM/CHS, followed by exchange to the detergent of choice on the ligand-affinity column.

Fig. 6BC displays SEC chromatograms for different detergents such as common maltosides like DDM and DM, and neopentyl glycosides like LMNG, UDMNG and DMNG. Noteworthy, the addition of CHS to the detergent in a 1:10 weight ratio always increased the size of the micelles, while reducing the hydrophobic chain length made the micelles smaller.

LMNG leads to a relatively small size of the protein-detergent complex and very good long-term stability. Because of the intended use in NMR, only detergents that resulted in small protein-micelle complexes, comparable to LMNG or smaller, were tested for long-term stability. In DMNG the receptor could be purified in good yields but aggregated after incubation for 3 days at 47 °C, even in the presence of CHS. In DH_7PC, the yields after receptor purification were very low, and the corresponding peak in SEC was broad, and no active receptor remained after 1 day at 37 °C. In UDMNG, the receptor displayed almost comparable stability as in LMNG. However, the size-difference was only minor and LMNG still displayed superior stability. Therefore, LMNG was the detergent of choice moving forward. Compared to the mutant #12, the stability of mutant B1 was significantly higher. After 15 days at 47 °C almost no aggregation was visible, while > 50% of mutant #12 was aggregated. Importantly, this high stability could only be achieved in the prazosin-bound state, while the apo state sustained well only temperatures up to 22 °C.

2.7. Incorporation into lipid nanodiscs

Detergents are artificial membrane mimetics that do not fully reflect the lipid bilayer, especially when they have very short alkyl chains. Lipid nanodiscs, on the other hand, represent a more natural environment for solubilizing membrane proteins, since they form planar bilayers. Nanodiscs are composed of two copies of a membrane scaffold protein (MSP), which are wrapped around a lipid bilayer, forming small disk-shaped objects. By changing the length of the MSP, disks of different sizes are obtained. This technique was developed by Sligar et al. [21], and MSP constructs yielding smaller nanodiscs were developed by Hagn et al. [22]. In our hands, best results were obtained with the MSPΔH5 construct and the circularized version, the cNW9 [23], where the N- and C-termini are covalently fused using sortase-mediated ligation.

To incorporate the receptor into the nanodiscs, a mixture of detergent-solubilized receptor, detergent-solubilized lipids and MSP was incubated at a chosen temperature. The detergent was removed with BioBeads, triggering formation of the receptor-nanodiscs complexes, provided that an optimal lipid:MSP:receptor ratio was achieved.

Many different conditions were screened for receptor incorporation into nanodiscs. The receptor was purified in different detergents such as DM, DDM, and LMNG, and incorporation was tested for different lipids (DMPC, DMPG, POPC and POPG) at different temperatures, ratios and amounts of BioBeads. Finally, one condition was identified that allowed incorporation yields of approximately 78%. The optimized protocol used the lipid mixture DMPC:DMPG in a 3:2 molar ratio solubilized in Na-cholate, the receptor solubilized in a low concentration of LMNG (~0.02%), an incubation temperature of 25 °C and a receptor:MPSΔH5:lipid molar ratio of 1:8:400 (or 1:8:480 for cNW9). The same protocol was also successful for a lipid mixture containing CHS in a ratio DMPC:DMPG:CHS of 3:2:1.

The incorporation of the α_{1B}-AR into the circularized version of the scaffold protein used the same protocol and resulted in similar yields. After incorporation and purification, the scaffold protein and the receptor could both be detected on the SDS-PAGE gel (Fig. S5) and showed a single peak with the expected size on the SEC chromatogram. The long-term stability was tested at 47 °C for both nanodisc samples, showing a slightly better stability in the cNW9 nanodiscs. However, in comparison to LMNG micelles the long-term stability in the nanodiscs was slightly inferior (Fig. 7).

NMR spectra could be measured for the α_{1B}-AR-B1D1-His construct, since the receptor-nanodisc assemblies could be separated from the empty nanodiscs by His-trap pulldown. Removal of empty nanodiscs was crucial because too high concentrations of empty nanodiscs resulted in complete sample aggregation at higher temperatures. Incorporation with high yields could only be achieved with the prazosin-bound receptor and not with the significantly less stable apo-state receptor.

2.8. Initial NMR experiments

The quality of NMR spectra is of prime importance to allow successful assignments. It is a common experience that spectra of helical membrane proteins display inferior quality when compared to those of well-behaved soluble proteins. The detergent micelle or lipid nanodiscs add to the apparent molecular weight of the protein slowing down tumbling rates, and hence even rigid membrane proteins display broader lines than soluble proteins of comparable size. The effects of transverse relaxation can be somewhat reduced by perdeuteration that serves to dilute protons and thereby removes many sources of dipolar interaction. A representative [^{15}N,^{1}H]-TROSY spectrum of the α_{1B}-AR-B1D1 in LMNG micelles is depicted in Fig. 8.

In general, line-shapes and peak intensities are of reasonable to good quality. However, some signals display unusual line-shapes, indicating the presence of more than one conformation. A count of the peaks, however, immediately reveals that too few signals are observed in the [^{15}N,^{1}H]-TROSY spectrum of the α_{1B}-AR construct.

The missing peaks could be absent because they may be broadened beyond detection by conformational exchange processes. 7-TM proteins, and in particular GPCRs, populate various states, and transitions between these occur frequently as part of their biological function. Stabilizing the inactive state by directed evolution and by binding to a high-affinity antagonist (prazosin), however, should have reduced conformational exchange processes.

Another explanation for the missing peaks is a lack of back-exchange of amide deuterons to protons. Triple-resonance 3D NMR spectra of helical membrane proteins require perdeuterated samples to reduce transverse relaxation to tolerable levels. Especially the Cα needs to be fully deuterated to allow experiments involving transfer steps or chemical shift labeling of Cα. Deuteration is usually obtained by expressing in deuterated water, and hence all amide protons are replaced by deuterons as well and need to be exchanged back to protons during purification. Unfortunately, water never gains access to most amides of the TM helices, and therefore amide deuterons cannot easily be exchanged back to detectable protons. In principle, this problem could be circumvented if the protein is unfolded and then refolded, which however proved so far to be impossible for the α_{1B}-AR.

To verify that the missing peaks were indeed due to the lack of back-exchange, the α_{1B}-AR-B1D1 construct was expressed in light water, and a spectrum of a highly concentrated sample was compared to the spectrum recorded with a sample expressed in deuterated water (Fig. 8). Peaks in the protonated spectra are broader and hence weaker than in the deuterated sample, but many additional peaks appeared. To verify the hypothesis that the lack of some peaks in the deuterated sample is due to missing back-exchange, the buffer of the protonated sample was exchanged to a pure D_2O buffer. Fig. 8 demonstrates that the additional peaks in the sample that stem from expression in light

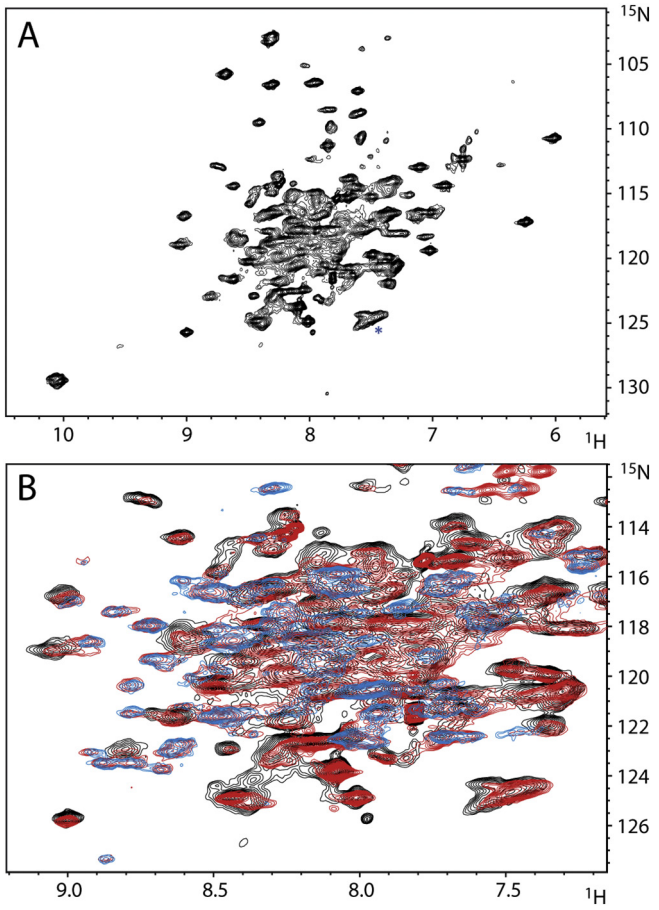

Fig. 8. Heteronuclear NMR spectra of the α_{1B}-AR-B1D1 in LMNG. **A** [^{15}N,^{1}H]-TROSY of 300 μM deuterated α_{1B}-AR-B1D1. **B**: Expansion of the [^{15}N,^{1}H]-TROSY spectra of the receptor expressed in D_2O (black; 250 μM) and in H_2O (red; 400 μM). Blue contours shows the protonated sample after exchange to pure D_2O buffer. All spectra were recorded at 700 MHz, 47 °C. (For interpretation of the references to colour in this figure legend, the reader is referred to the web version of this article.)

water did not disappear in the D_2O buffer. This was a clear indication that these amide protons are protected from water access. Interestingly, after recording 3D spectra for many days at 47 °C some additional peaks appeared in the 2D spectra, likely from amides with very slow exchange with water.

In addition, we also recorded [^{15}N,^{1}H]-TROSY spectra of the α_{1B}-AR-B1D1-His construct in DMPG/DMPC nanodiscs (Fig. 9). The quality of the spectrum in the smaller LMNG micelle is significantly better than the corresponding one in the nanodiscs. The ^{15}N—^{1}H correlation spectra are different, which is not surprising, considering that only water-accessible parts can be seen. These regions are likely in contact or close to the headgroup of the detergent or the lipid, and therefore have a different chemical environment.

The detection of methyl groups in [^{13}C,^{1}H]-HSQC spectra is much more sensitive than detection of amide moieties in the corresponding ^{15}N-correlated spectra due to the rotation of the methyl group about its symmetry axis, and the fact that there are three homotopic protons. The methyl spectra in LMNG and nanodiscs look more similar and all expected peaks are likely visible, because they do not suffer from the lack of back exchange. Since methyl groups rarely face the lipid headgroups, differences between nanodiscs and detergent micelles are smaller and peaks in general shift only slightly. It should be kept in mind that different chemical shifts could arise from a different distribution of conformations of the receptor in nanodiscs and in detergent micelles as reported from Kofuku et al. [24].

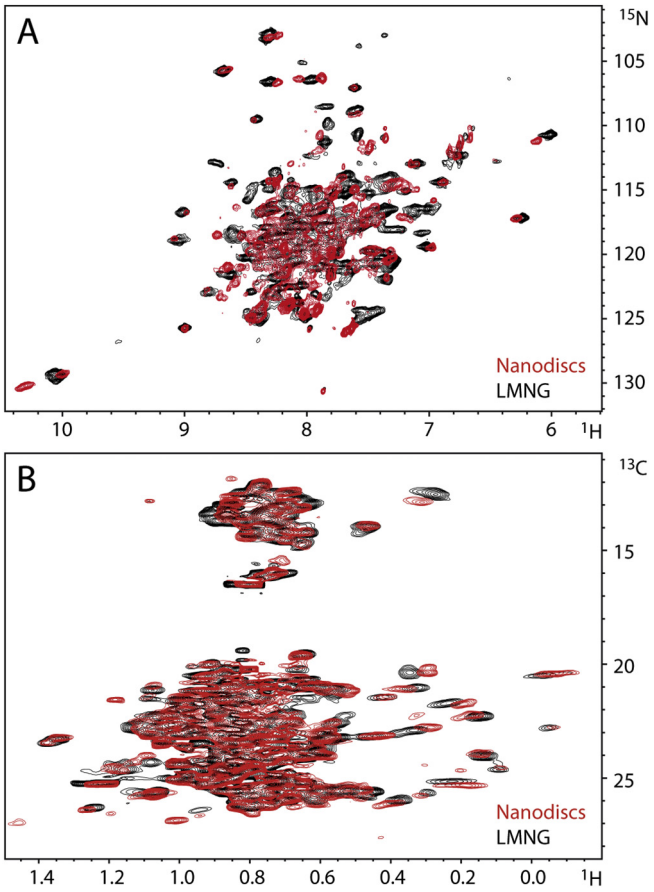

Fig. 9. Comparison of heteronuclear NMR spectra of α_{1B}AR-B1D1 in LMNG micelles and α_{1B}AR-B1D1-His in nanodiscs. **A** [^{15}N,^{1}H]-TROSY of 180 μM B1D1-His in nanodiscs and 250 μM B1D1 in LMNG. **B** [^{13}C,^{1}H]-HSQC of 180 μM B1D1-His in nanodiscs and 300 μM B1D1 in LMNG. Spectra were recorded at 700 MHz, 47 °C.

3. Discussion

Understanding the dynamics of GPCRs is of prime importance to fully comprehend the molecular processes by which these receptors function. X-ray crystallography and cryo-EM have provided much molecular detail describing structures of GPCRs in various states and in complex with signaling partners [2], but these represent frozen snapshots of certain states. Since it is well established that GPCRs populate multiple states, interconversion between these populations are fundamental for receptor activation [4]. In principle, solution NMR is a technique suitable to analyze these dynamical processes, but problems arise in obtaining spectra of sufficient quality to allow assignment of the corresponding peaks. In recent years, many NMR studies performed on GPCRs focused on specific aspects of receptor activation or interaction with ligands, G proteins or arrestins [25]. Whether it is structure calculations, chemical shift perturbations or determination of dynamics, chemical shift assignments are usually the first step in the analysis. When using proteins of the size of a GPCR, assignment methods that are not based on mutagenesis require samples with high deuteration of non-labile protons, and often methyl-protonated proteins in fully perdeuterated background are particularly useful. The best host to accomplish such labeling patterns is currently *E. coli*.

Unfortunately, GPCRs generally do not express well in *E. coli*, a host for which uniform ^{15}N and ^{13}C labeling strategies as well as the important deuteration are well established. Therefore, expression has been usually performed in insect cells, and only a certain type of amino acid was selectively labeled, for example with ^{19}F probes attached to cysteines [26,27] or $^{13}CH_3$-Met [28–30] and assigned by mutagenesis [31]. These sensitive probes give useful spectra even without perdeuteration, albeit only at individual positions. The β_1-AR and the β_2-AR could be labeled with ^{15}N-Val and ^{15}N-Leu, respectively. Assignments were obtained by point mutations and chemical shift perturbations could be measured [32]. Nevertheless, three receptors have been expressed in *E. coli* for NMR measurements. The BLT2 receptor was expressed as inclusion bodies in *E. coli* and could successfully be refolded into nanodiscs [33]. In addition, NTR1 stabilized by CHESS and thus expressible as a functional protein in *E. coli* was investigated [23,34]. In a recent NMR study a highly stabilized version of the α_{1A}-AR was modified to enable signaling, and expressed in *E. coli* with $^{13}CH_3$-methionine labeling [31]. An elegant way of combining *E. coli* expression with insect cell expression was shown by Shiraishi et al. [35], where the C-terminal portion following helix 8 of the β_2-AR was expressed and labeled in *E. coli* and then fused through protein trans-splicing to a $^{13}CH_3$-Met labeled receptor that was produced in insect cells. Methods that use insect or mammalian cells unfortunately significantly restrict the tools for isotope-labeling [36]. Presently, a severe disadvantage is the fact that ILV methyl labeling in perdeuterated background is impossible because these cells cannot be grown in deuterated water and the established ILV precursors are not metabolized in these cells. The measurement of methyl dynamics, however, strictly requires *almost complete* absence of protons proximal to the methyl groups, and this is most conveniently achieved in *E. coli*. Nonetheless, *P. pastoris* is a eukaryotic host which allows deuteration. In these cells, the adenosine A_{2A} receptor was expressed with a deuteration level of 70% and even $^{13}CH_3$-Ile groups could be labeled with precursors [37,38].

To achieve a more extensive assignment and to probe the entire receptor by NMR, we uniformly labeled the GPCR and attempted to assign the peaks using standard triple-resonance NMR spectra. To overcome the low yields of heterologous expression of most wild-type GPCRs in *E. coli*, we used a directed evolution mutagenesis approach (CHESS method) [9] to obtain a well-expressing and stabilized mutant. Furthermore, we tested and analyzed many conditions to obtain a sample with the properties suitable for measuring 3D NMR spectra.

So far, the only 7-helical membrane protein structures determined by solution NMR techniques were proteorhodopsin [39] and sensory-rhodopsin [40], two microbial rhodopsins, which were both expressed in *E. coli* and solubilized in DH_7PC. In both cases extensive backbone and methyl assignments were made and good-quality structures were computed from NOEs and paramagnetic relaxation enhancement (PRE) probes. However, even with our stabilized GPCR mutant, we realized that the stability in the short-chain detergent DH_7PC was not sufficient to record NMR spectra over extended periods of time at elevated temperatures, and therefore, we had to use milder detergents which result in larger micelles. Recently, we could demonstrate that 62% of the backbone of bacteriorhodopsin can be assigned in large systems such as nanodiscs, indicating that the size of such proteins per se is not prohibitively large [41]. The quality of NMR spectra for the α_{1B}-AR incorporated into nanodiscs was unfortunately significantly inferior compared to samples in LMNG micelles, which, nonetheless, could be due to the increased size.

GPCRs are intrinsically dynamic proteins — they populate multiple conformations belonging to different activation states, and addition of ligands typically redistributes these populations. Thermostabilizing the receptors likely alters those dynamics, which makes many of them accessible to structural studies in the first place, as only extremely few natural ones intrinsically have the necessary stability. Nonetheless, great care must be taken to avoid overinterpretation by taking into account the likely changes in dynamics and redistribution of populations. Therefore, it is important to verify that the receptor mutant still has wild-type like behavior. In the end, most GPCRs cannot be investigated by NMR without addition of mutations or modifications. An exception is the adenosine A_{2A} receptor which seems to be a naturally more well-behaving receptor, and therefore NMR studies could be

carried out with a construct that contained no thermostabilizing mutations [26,37,38,42–46]. The investigated β_1-AR constructs usually contained a variety of different thermostabilizing mutations [29,32,45,47–49]. While the investigated β_2-AR variants in general contained fewer thermostabilizing mutations, they usually had mutations to reduce the number of Cys or Met residues [24,27,28,33,50–54]. In summary, most of the studied GPCRs have been optimized by mutations. We are convinced that a large fraction of GPCRs will only become amenable to detailed biophysical analysis once they are suitably stabilized. Our approach, starting with highly stabilized versions and subsequently removing some of these mutations to recover activity, presents a rational approach that is a powerful alternative to the presently used methods. The used α_{1B}-AR-B1 mutant did not show any signaling in an IP1-based signaling assay (data not shown) [55]. However, this receptor mutant helped to establish a protocol for the expression and purification, to optimize NMR experiments and to obtain initial assignments. In an ongoing study we recently obtained a stable and signaling-competent α_{1B}-AR receptor mutant (data not shown), which would not have been possible without the initial B1 mutant. In a similar approach, conformational changes observed in a signaling-incompetent α_{1A}-AR mutant, which could be used for establishing all expression and NMR methods, were essentially retained in the signaling-competent receptor [31], suggesting that the study of such stabilized mutants is very valuable.

An important remaining issue for the NMR analysis is the absence of amide peaks from the TM portions due to the lack of amide-proton back-exchange. So far, we were unable to develop conditions that lead to the back-exchange of these amide protons in the hydrophobic core. Amide protons are crucial for structure determinations because they serve as anchoring points for the sequential backbone assignment with 3D-spectra. Fortunately, *E. coli*, in contrast to eukaryotic expression hosts, allows production of perdeuterated proteins that incorporate fully protonated methyl groups, the so-called ILV labeling [56,57]. These methyl groups are ubiquitous in membrane proteins, in the α_{1B}-AR-B1 construct about one third of all amino acids. Experiments to use these probes for measuring side chain dynamics in membrane proteins have been developed that are tailored to this labeling pattern [9,58,59] but require absence of protons in the proximity of the methyl group. Methyl-based signals are detected much more sensitively than their amide-based counterparts. Our previous assignment of methyl groups in bacteriorhodopsin was heavily based on assigned backbone amides. However, it might be possible to assign the majority of the methyl groups with a 4D-NOESY and the help of an existing structure or a structure model and a few mutations. To obtain a high quality 4D-NOESY spectrum the receptor as well as the membrane mimetics need to be highly deuterated. The signal overlap, as apparent in Fig. 9B, can be drastically decreased if the spectra are recorded on a high field spectrometer ($\geq$900 MHz) and when using precursors for stereospecific labeling [57] (Fig. S6). A few mutations as anchoring points may still be required, but we believe that the required number of these is still much lower than for the so-far-used full mutagenesis approaches that are needed for GPCRs expressed in eukaryotic cells. We therefore anticipate that expression of GPCRs in *E. coli* will provide a useful avenue for obtaining these long-sought dynamics data.

4. Methods

4.1. Cloning

Receptor constructs were ordered as gBlock gene fragments (IDT) and cloned into the pRG (pBR322-derived) vector, with an N-terminal MBP and a C-terminal TrxA fusion, using the restriction enzymes BamHI and *Xma*I.

4.2. Expression

Competent *E. coli* BL21 cells (C2530, New England Biolabs) were transformed and selected on LB-agar containing 1% D(+)-glucose and 100 mg/L carbenicillin. A preculture from a single clone was grown in M9 H_2O media (3 g/L KH_2PO_4, 7.5 g/L $Na_2HPO_4 \cdot 2\ H_2O$, 0.5 g/L NaCl, 2 mM $MgSO_4$, 100 mg/L ampicillin, 1 mL/L 1000× trace metals (for composition see SI Supplementary Methods), 1.5 g/L [^{15}N]-NH_4Cl, 7 g/L D(+)-glucose, 100 mg/L yeast extract). For the expression in H_2O the main culture consisted of the same media without the yeast extract. At an OD_{600} = 0.8, the cells were induced with 0.5 mM IPTG (final concentration) and the expression was continued at 30 °C for 14–20 h.

For expression in deuterated media, a second preculture in M9 D_2O (3 g/L KH_2PO_4, 6 g/L Na_2HPO_4, 0.5 g/L NaCl, 2 mM $MgSO_4$, 100 mg/L ampicillin, 1 mL/L 1000× trace metals, 1.2 g/L [^{15}N]-ND_4Cl, 3.5 g/L D(+)-glucose-1,2,3,4,5,6,6-d_7) was inoculated from the M9 H_2O preculture. Receptor expression in the M9 D_2O main culture was as described above.

For the ILV labeling, the following precursors from Cambridge Isotope Laboratories were added 1 h before induction: 70 mg/L alpha-ketobutyric acid, sodium salt (methyl-^{13}C, 99%; 3,3-D_2, 98%) and 160 mg/L alpha-ketoisovaleric acid, sodium salt (3-methyl-^{13}C, 99%; 3,4′,4′,4′-D_4, 98%).

For the stereoselective ILVproS labelling, the following precursors from NMR-Bio were added according to the manufacturer's instructions: 1 h before induction 2-hydroxy-2-[2′-^{13}C,^{1}H-1′-D_2]ethyl-3-oxo-4[D_3] butanoic acid and 20 min before induction 2-(D_3) methyl, 2,4-($^{13}C_2$,^{1}H)-acetolactate.

4.3. Purification

The purification was performed at 4 °C with precooled buffers. Cells were resuspended in 7.5 mL/g pellet of 50 mM HEPES pH 8, 200 mM NaCl, 10% glycerol, 15 mM imidazole, 2 mg/mL lysozyme, 0.05 mg/mL of DNase and 5 mM $MgCl_2$. A mixture of 10% (w/v) n-dodecyl-β-D-maltopyranoside (DDM, Anatrace) and 1% (w/v) cholesteryl hemisuccinate (CHS, Sigma-Aldrich) was added to a final concentration of 2% DDM / 0.2% CHS and solubilization was continued for 2 h with stirring. The lysate was centrifuged for 30 min at 18,000 rpm in a SS34 rotor. The supernatant was incubated with TALON Superflow resin (GE Healthcare) equilibrated with TWB1 (25 mM HEPES pH 8, 600 mM NaCl, 10% glycerol, 0.075% lauryl maltose neopentyl glycol (LMNG, Anatrace), 15 mM imidazole). Per 1 g of cells 1 mL of TALON resin was used and the binding was continued for 2.5 h with gentle rolling. Washing was performed in PD10 columns with a column volume (CV) of 2.5 mL TALON resin. The columns were washed 4 times with 4 CV of TWB1 and 4 times with 4 CV of TWB2 (25 mM HEPES pH 7, 150 mM NaCl, 10% glycerol, 0.05% LMNG). The protein was eluted with 3 CV of TEB (25 mM HEPES pH 8, 150 mM NaCl, 10% glycerol, 0.05% LMNG, 200 mM EDTA). 1 mg of 3C protease was added per 15 mL of elution and incubated for 30 min. Per 5 g of cells 0.5 mL of prazosin column (PC) resin equilibrated in TEB was added and incubated overnight. The resin was subsequently transferred into an empty PD10 or a 2 mL Bio-Rad column and was washed 3 times with 2 CV of PCWB1 (25 mM HEPES pH 8, 600 mM NaCl, 10% glycerol, 0.025% LMNG, 200 mM EDTA) and 3 times with 2 CV of PCWB2 (20 mM Na-Phosphate pH 7, 20 mM NaCl, 0.01% LMNG). 4.5 CV of PCEB (10 mM Na-phosphate pH 7, 20 mM NaCl, 0.01% LMNG, 85 μM prazosin (Sigma-Aldrich)) was added to the column and incubated while rolling for 2 h. The flow-through as well as a wash with two times 1 CV of PCEB were collected. The final protein sample was obtained by concentrating the PC elution using an Amicon Ultra-4 (50 kDa molecular weight cut-off).

In order to determine the protein concentration, excess prazosin had to be removed. To this end, an analytical fraction of the final sample was loaded onto a Zeba Spin desalting column (7 kDa molecular weight cut-off, Thermo Fisher Scientific) equilibrated with 10 mM Na-

phosphate pH 7, 100 mM NaCl, 0.01% LMNG, 2.5 μM prazosin. Absorption at 280 nm was measured using a Nanodrop spectrophotometer and it was corrected with an empirically determined correction factor of 0.7 to take into account absorption of receptor-bound prazosin.

To obtain the apo receptor, elution from the PC was performed in 10 mM Na-phosphate pH 7, 20 mM NaCl, 0.01% LMNG, 350 mM imidazole. Imidazole was then removed with a PD-10 desalting column (GE Healthcare) and by dialysis in a 10 mL Float-A-Lyzer (Spectrum) with a 10 kDa molecular weight cut off against 500 mL of 10 mM Na-phosphate pH 7, 20 mM NaCl, 0.01% LMNG.

4.4. Reconstitution of α_{1B}-AR into nanodiscs

Deuterated lipids d_{54}-DMPC and d_{54}-DMPG (from FB reagents) were solubilized at 50 mM in Lipid buffer (20 mM HEPES pH 8, 100 mM Na-cholate) at 47 °C and a lipid mix of DMPC:DMPG at a molar ratio of 3:2 was prepared. The purified constructs α_{1B}-AR-B1D1-His at 2 mg/mL in LMNG, MSPΔH5 at 3.5 mg/mL and the lipid mix were mixed in a molar ratio of 1:8:400 (or 1:8:480 for cNW9) and incubated overnight at 25 °C and 600 rpm. 0.5 g/mL prewarmed BioBeads SM-2 (Bio-Rad) were added to the mix and incubated for 4 h at 25 °C with slight shaking. The BioBeads were removed by filtration and washed two times with 5 mL of α_{1B} Nanodisc buffer (20 mM Tris pH 8 at RT, 100 mM NaCl, 10 μM prazosin). The flow-through was collected and prazosin was added to a final concentration of 20 μM. The nanodisc solution was loaded on a 1 mL HisTrap HP column (GE Healthcare) and washed with α_{1B} Nanodisc buffer. The α_{1B}-AR nanodiscs were eluted with 20 mM Tris pH 8, 100 mM NaCl, 300 mM imidazole, 20 μM prazosin. The elution was buffer-exchanged with a PD-10 desalting column to 10 mM Na-phosphate pH 7, 20 mM NaCl, 10 μM prazosin and subsequently concentrated to 200 μL using an Amicon Ultra-4 (50 kDa molecular weight cut-off). Additional information for the purification of MSPΔH5 and cNW9 is described in the SI.

4.5. SDS-PAGE

The protein samples were analyzed on 8–16% ExpressPlus PAGE Gels (GenScript) with 1× Tris-MOPS buffer (50 mM Tris, 50 mM MOPS 0.1% SDS, 1 mM EDTA) in a Biorad electrophoresis system. 20 μL of the protein sample was mixed with 6.6 μL 4× SDS loading buffer (200 mM Tris pH 6.8, 400 mM DTT, 8% SDS, 0.4% bromophenol blue, 40% glycerol) and stored at −20 °C until further use. The samples were not heated up prior to loading because heating the samples led to laddering of the receptor on the gel. The gel was run for 45 min at 140 V. Afterwards, the gel was stained for 15–60 min with staining buffer (40% methanol, 10% acetic acid, 2.4 g/L Coomassie brilliant blue R-250). The background was destained 2–3 times with destaining buffer (40% methanol, 10% acetic acid) for 15–30 min. The gel was imaged using a Biorad ChemiDoc MP imaging system.

4.6. Fluorescent ligand-based stability assay

20 g of cells after expression were resuspended in 80 mL of PBS and 10 mL aliquots were stored at −80 °C. One aliquot was mixed with the same volume of PBS pH 7.4, 4 mg/mL lysozyme, 0.2 mg/mL DNase, 1 mM EDTA, 1 tablet of Roche cOmplete mini protease inhibitors, 4% DM and 0.8 μM BODIPY-FL-prazosin. For the background control, another aliquot was mixed with the same buffer supplemented with 0.2 mM prazosin. Both aliquots were incubated for 2 h at 4 °C while rotating. Cell debris was pelleted with a Fiberlite SLA600TC rotor at 13,000 rpm for 30 min at 4 °C. 500 μL Streptavidin-coupled Dynabeads were added to the supernatant and incubated for 1 h at 4 °C. 200 μL of the Dynabeads suspension was added to each well of a KingFisher 96 well-plate. The beads were washed 2 times with a KingFisher robot in 300 μL of 50 mM Na-phosphate pH 7.4 supplemented with either one of the following detergents: DPC 5 mM, LMPC 1 mM, LMPG 1 mM, LPPG 1 mM, DH_6PC 30 mM, DH_7PC 4 mM, LMNG 0.01%, LMNG/CHS 0.01/0.001%, DDM 0.1%, DDM/CHS 0.1/0.01%, DM 0.5%, DM/CHS 0.5/0.05%, LDAO 5 mM, Tween20 0.02%. The beads were transferred in 140 μL of the detergent buffer containing either 0.25 μM BODIPY-FL-prazosin or an additional 12.5 μM prazosin for the background control. Two plates with the same conditions were prepared and sealed. One was incubated for 1 h and the other for 24 h at 37 °C while shaking at 1000 rpm. After the incubation, the beads were washed again 2 times in 300 μL of the corresponding detergent buffer and transferred in 120 μL thereof. 100 μL of the suspension was transferred in a black 96-well plate on ice and the fluorescence was measured (excitation 458 nm, emission 520 nm).

4.7. Radioligand binding assay

After expression, 100 μL aliquots of bacterial culture were pelleted for 10 min at 10,000 ×*g* at room temperature. The supernatant was carefully removed, and the cell pellets were flash-frozen in liquid nitrogen and stored at −80 °C.

The samples were resuspended in Wash buffer (50 mM Tris-HCl pH 7.4) to an OD_{600} of 1. In a 96-well plate, 20 μL of the cell suspension was added to 160 μL of binding buffer (50 mM Tris-HCl pH 7.4, 1 mM EDTA pH 8, 40 μg/mL Bacitracin, 0.1% (w/v) BSA, 20 nM ^{3}H-prazosin (PerkinElmer) or binding buffer supplemented with 40 μM prazosin. The plate was closed with an adhesive seal and incubated for 2–3 h at 4 °C while shaking. Meanwhile, a 96-well filter plate was incubated with 200 μL of 0.5% polyethyleneimine (PEI) at room temperature for 2–3 h. The PEI solution was removed by a vacuum pump and the plate was washed two times with 280 μL of Wash buffer. 120 μL of each sample was added to the filter plate and the liquid was removed by vacuum. The plate was washed 4 times with 200 μL of Wash buffer and the filters were transferred into a 96-well Isoplate (PerkinElmer). The filters were dried for 1 h at 65 °C, incubated overnight with 200 μL of Optiphase Supermix (PerkinElmer) at room temperature and the radioactivity was measured in a liquid scintillation counter (PerkinElmer Microbeta 1450 plus). The concentration of ligand-bound receptor was calculated according to reference filters with a known concentration of hot ligand. The number of receptors per cells were estimated from the OD_{600}, assuming that 1×10^9 cells per mL refer to an OD_{600} of 1.

To determine the K_d values, the incubation was performed with binding buffers containing different concentrations of ^{3}H-prazosin (0.01–20 nM). The resuspended cells were added to an OD_{600} of 0.02 for the stabilized receptor mutants and to 0.2 for the WT receptor. The calculations were performed using R version 3.3.3. Expected background signals, as measured by competition assays, were estimated by linear regression with the intercept set to zero, and were subtracted from the signal of the samples. Reference samples were used to calculate a standard curve to correlate cpm/fmol by linear regression with the intercept set to zero. K_d values were estimated using a non-linear least squares approach using the following model derived from the K_d definition:

$$Y = (B_{max} \bullet X)/(K_d + X)$$

B_{max} (total concentration of receptor) and K_d were optimized to fit the curve. Y is the concentration of bound ligand and X is the concentration of free ligand, calculated by subtracting Y from the total ligand concentration.

4.8. CPM assay

The purified receptor in DDM/CHS was diluted to a final concentration of 1–2 μM in CPM dilution buffer (10 mM HEPES pH 7.5, 100 mM NaCl, 10% glycerol, 0.025% (w/v) DDM, 0.005% (w/v) CHS), 20 μM prazosin). The fluorescent dye 7-diethylamino-3-(4-

maleimidophenyl)-4-methylcoumarin (CPM, Sigma), dissolved to 10 mM in DMSO, was diluted 40-fold to 250 μM with CPM dilution buffer and was kept on ice and in the dark until use.

The diluted CPM dye was added to the receptor sample to a final concentration of 25 μM. 20 μL of the mixture was transferred into a 96-well plate for an Agilent MX3005p qPCR reader, sealed with adhesive foil and incubated for 15 min at 25 °C. Each experiment was measured as a triplicate. The fluorescence signal was monitored (excitation 387 nm, emission 463 nm) while increasing the temperature by 2 °C per min from 25 °C to 95 °C.

4.9. SEC thermostability assay

The receptor was concentrated to approximately 2–3 mg/mL and 100–200 μL were filled into a 1.5 mL screw cap tube. The tube was sealed tightly with parafilm and put in a 5 mL Eppendorf tube filled with 100 μL water, to minimize evaporation. After incubation in an Eppendorf thermoshaker at 700 rpm or in a Binder incubator, aggregates were removed by spinning for 5 min at maximum speed in an Eppendorf MiniSpin. 13 μL of the supernatant was filled into a 2 mL screw cap glass vial with conical bottom and loaded with an Agilent 1260 Infinity HPLC system onto a Superdex 200 increase 10/150 column. Additionally, a Wyatt miniDAWN TREOS detector and a Shodex RI-101 detector were connected to the system. The chromatography run was monitored with Agilent ChemStation software and Astra software from Wyatt, collecting data for UV at 280 nm and 340 nm, refractive index and multiangle light scattering. The protein could be followed at 280 nm, the presence of prazosin could be measured at 340 nm and the refractive index was used as a quality control on the buffer salt peak to see if the sample might have been concentrated through evaporation.

4.10. SEC-MALS measurements

The SEC-MALS measurements were performed on a Superdex 200 Increase 10/300 column on an Agilent 1260 Inifinity HPLC system with a Wyatt miniDAWN TREOS and a Shodex RI-101 detector in 20 mM Na-phosphate pH 7, 100 mM NaCl and 0.01% (w/v) LMNG or 0.05% (w/v) DDM/0.005% (w/v) CHS. The measurement was carried out at room temperature with a flow rate of 0.5 mL/min. The protein and detergent masses were calculated with the Astra 6 program from Wyatt. The light scattering detector miniDAWN TREOS was calibrated with toluene and the refractive index detector Shodex RI-101 was calibrated manually with a BSA run. The extinction coefficient of the protein was calculated with the ExPASy ProtParam tool, and the standard dn/dc value for proteins of 0.185 mL/g was used. For the detergents the dn/dc values were measured by manually injecting 5 mL of a 0.1%, 0.2%, 0.3%, 0.4% and 0.5% (w/v) detergent solution in water into the Shodex RI-101 detector. The dn/dc values were then calculated with the Astra 6 program from Wyatt. The detergents alone also absorb slightly at 280 nm, therefore an extinction coefficient of 0.012 mL/(mg·cm) was empirically determined by analyzing the DDM/CHS micelle peak.

4.11. MS measurements

50 μL of 1–2 mg/mL receptor in LMNG was precipitated with TCA at 4 °C and was centrifuged at 12,000 $\times g$ for 10 min. The supernatant was discarded, and the pellet was washed twice with acetone at −20 °C. The pellet was reconstituted in hexafluoroisopropanol (HFIP) with 1% formic acid and diluted with HFIP/isopropanol/formic acid and analyzed by ESI-MS in a mass range between 50 and 5000 Da. The sampling cone energy was set to 100–150 V. The *m/z* data were deconvoluted using MaxEnt1 with an output resolution of 1 Da.

4.12. NMR measurements

NMR measurements were performed on a Bruker Avance 700 MHz spectrometer with a cryogenically cooled TXI probe head at the UZH. Samples were concentrated to approximately 200–400 μM in 10 mM Na-phosphate pH 7, 20 mM NaCl, 10% D_2O, an excess of 85 μM prazosin and a final concentration of approximately 0.6% LMNG. Fully protonated and d_{42}-LMNG (FG Reagents) were used for nitrogen and carbon correlations, respectively. All proton chemical shifts were referenced to the water line at 4.48 ppm at 47 °C, from which the nitrogen and carbon scales were derived indirectly by using the conversion factors of 0.10132900 (^{15}N) and 0.25144954 (^{13}C). Experiments were recorded with the Bruker standard pulse sequences using sensitivity-enhanced [^{15}N,^{1}H]-TROSY and [^{13}C,^{1}H]-HSQC spectra. Spectra were processed and analyzed with TopSpin 4.0.

Declaration of competing interest

Herewith I declare that I have no competing interest concerning the paper entitled "**Optimizing the α_{1B}-Adrenergic Receptor for Solution NMR Studies**" submitted to *Biochimica et Biophysica Acta Biomembranes*.

Acknowledgments

This project is supported by a grant from the Swiss National Science Foundation (grant no. 310030_179314 to O.Z.) and from the Research Foundation of the University of Zurich (grant no. FK-18-083 to C.B.). We deeply thank Franz Hagn for a gift of the MSPΔH5 expression plasmid.

Appendix A. Supplementary data

Supplementary data to this article can be found online at https://doi.org/10.1016/j.bbamem.2020.183354.

References

[1] K. Sriram, P.A. Insel, GPCRs as targets for approved drugs: how many targets and how many drugs, Mol. Pharmacol. (2018) 251–258.
[2] D. Hilger, M. Masureel, B.K. Kobilka, Structure and dynamics of GPCR signaling complexes, Nat. Struct. Mol. Biol. 25 (2018) 4–12.
[3] D. Wootten, A. Christopoulos, M. Marti-Solano, M.M. Babu, P.M. Sexton, Mechanisms of signalling and biased agonism in G protein-coupled receptors, Nat. Rev. Mol. Cell Biol. 19 (2018) 638–653.
[4] N.R. Latorraca, A.J. Venkatakrishnan, R.O. Dror, GPCR dynamics: structures in motion, Chem. Rev. 117 (2017) 139–155.
[5] A.J. Venkatakrishnan, X. Deupi, G. Lebon, C.G. Tate, G.F. Schertler, M.M. Babu, Molecular signatures of G-protein-coupled receptors, Nature 494 (2013) 185–194.
[6] B.K. Kobilka, G protein coupled receptor structure and activation, Biochim. Biophys. Acta 1768 (2007) 794–807.
[7] R. Nygaard, T.M. Frimurer, B. Holst, M.M. Rosenkilde, T.W. Schwartz, Ligand binding and micro-switches in 7TM receptor structures, Trends Pharmacol. Sci. 30 (2009) 249–259.
[8] L. Ragnarsson, Å. Andersson, W.G. Thomas, R.J. Lewis, Mutations in the NPxxY motif stabilize pharmacologically distinct conformational states of the α_{1B}- and β_2-adrenoceptors, Sci. Signal. 12 (2019) eaas9485.
[9] D. Sheppard, R. Sprangers, V. Tugarinov, Experimental approaches for NMR studies of side-chain dynamics in high-molecular-weight proteins, Prog. Nucl. Magn. Reson. Spectrosc. 56 (2010) 1–45.
[10] C. Munk, E. Mutt, V. Isberg, L.F. Nikolajsen, J.M. Bibbe, T. Flock, M.A. Hanson, R.C. Stevens, X. Deupi, D.E. Gloriam, An online resource for GPCR structure determination and analysis, Nat. Methods 16 (2019) 151–162.
[11] D.J. Scott, L. Kummer, D. Tremmel, A. Plückthun, Stabilizing membrane proteins through protein engineering, Curr. Opin. Chem. Biol. 17 (2013) 427–435.
[12] D.J. Scott, A. Plückthun, Direct molecular evolution of detergent-stable G protein-coupled receptors using polymer encapsulated cells, J. Mol. Biol. 425 (2013) 662–677.
[13] K.J. Yong, T.M. Vaid, P.J. Shilling, F.J. Wu, L.M. Williams, M. Deluigi, A. Plückthun, R.A.D. Bathgate, P.R. Gooley, D.J. Scott, Determinants of ligand subtype-selectivity at α_{1A}-adrenoceptor revealed using saturation transfer difference (STD) NMR, ACS Chem. Biol. 13 (2018) 1090–1102.
[14] P. Egloff, M. Hillenbrand, C. Klenk, A. Batyuk, P. Heine, S. Balada, K.M. Schlinkmann, D.J. Scott, M. Schütz, A. Plückthun, Structure of signaling-

competent neurotensin receptor 1 obtained by directed evolution in *Escherichia coli*, Proc. Natl. Acad. Sci. U. S. A. 111 (2014) E655–E662.
[15] J. Tucker, R. Grisshammer, Purification of a rat neurotensin receptor expressed in *Escherichia coli*, Biochem. J. 317 (1996) 891–899.
[16] P. Egloff, M. Deluigi, P. Heine, S. Balada, A. Plückthun, A cleavable ligand column for the rapid isolation of large quantities of homogeneous and functional neurotensin receptor 1 variants from *E. coli*, Protein Expr. Purif. 108 (2015) 106–114.
[17] A.I. Alexandrov, M. Mileni, E.Y. Chien, M.A. Hanson, R.C. Stevens, Microscale fluorescent thermal stability assay for membrane proteins, Structure 16 (2008) 351–359.
[18] Z. Wang, C. Ye, X. Zhang, Y. Wei, Cysteine residue is not essential for CPM protein thermal-stability assay, Anal. Bioanal. Chem. 407 (2015) 3683–3691.
[19] X. Zhang, R.C. Stevens, F. Xu, The importance of ligands for G protein-coupled receptor stability, Trends Biochem. Sci. 40 (2015) 79–87.
[20] S. Igonet, C. Raingeval, E. Cecon, M. Pučić-Baković, G. Lauc, O. Cala, M. Baranowski, J. Perez, R. Jockers, I. Krimm, A. Jawhari, Enabling STD-NMR fragment screening using stabilized native GPCR: a case study of adenosine receptor, Sci. Rep. 8 (2018) 8142.
[21] T.H. Bayburt, S.G. Sligar, Membrane protein assembly into Nanodiscs, FEBS Lett. 584 (2010) 1721–1727.
[22] F. Hagn, M. Etzkorn, T. Raschle, G. Wagner, Optimized phospholipid bilayer nanodiscs facilitate high-resolution structure determination of membrane proteins, J. Am. Chem. Soc. 135 (2013) 1919–1925.
[23] M.L. Nasr, D. Baptista, M. Strauss, Z.J. Sun, S. Grigoriu, S. Huser, A. Plückthun, F. Hagn, T. Walz, J.M. Hogle, G. Wagner, Covalently circularized nanodiscs for studying membrane proteins and viral entry, Nat. Methods 14 (2017) 49–52.
[24] Y. Kofuku, T. Ueda, J. Okude, Y. Shiraishi, K. Kondo, T. Mizumura, S. Suzuki, I. Shimada, Functional dynamics of deuterated β_2-adrenergic receptor in lipid bilayers revealed by NMR spectroscopy, Angew. Chem. Int. Ed. Eng. 53 (2014) 13376–13379.
[25] M.J. Bostock, A.S. Solt, D. Nietlispach, The role of NMR spectroscopy in mapping the conformational landscape of GPCRs, Curr. Opin. Struct. Biol. 57 (2019) 145–156.
[26] L. Ye, N. Van Eps, M. Zimmer, O.P. Ernst, R.S. Prosser, Activation of the A_{2A} adenosine G-protein-coupled receptor by conformational selection, Nature 533 (2016) 265–268.
[27] J.J. Liu, R. Horst, V. Katritch, R.C. Stevens, K. Wüthrich, Biased signaling pathways in β2-adrenergic receptor characterized by ^{19}F-NMR, Science 335 (2012) 1106–1110.
[28] Y. Kofuku, T. Ueda, J. Okude, Y. Shiraishi, K. Kondo, M. Maeda, H. Tsujishita, I. Shimada, Efficacy of the β_2-adrenergic receptor is determined by conformational equilibrium in the transmembrane region, Nat. Commun. 3 (2012) 1045.
[29] A.S. Solt, M.J. Bostock, B. Shrestha, P. Kumar, T. Warne, C.G. Tate, D. Nietlispach, Insight into partial agonism by observing multiple equilibria for ligand-bound and G_s-mimetic nanobody-bound β_1-adrenergic receptor, Nat. Commun. 8 (2017) 1795.
[30] J. Xu, Y. Hu, J. Kaindl, P. Risel, H. Hübner, S. Maeda, X. Niu, H. Li, P. Gmeiner, C. Jin, B.K. Kobilka, Conformational complexity and dynamics in a muscarinic receptor revealed by NMR spectroscopy, Mol. Cell 75 (2019) 53–65.
[31] F.J. Wu, L.M. Williams, A. Abdul-Ridha, A. Gunatilaka, T.M. Vaid, M. Kocan, A.R. Whitehead, M.D.W. Griffin, R.A.D. Bathgate, D.J. Scott, P.R. Gooley, Probing the correlation between ligand efficacy and conformational diversity at the α_{1A}-adrenoreceptor reveals allosteric coupling of its microswitches, J. Biol. Chem. (2020), https://doi.org/10.1074/jbc.RA120.012842.
[32] S. Isogai, X. Deupi, C. Opitz, F.M. Heydenreich, C.J. Tsai, F. Brueckner, G.F. Schertler, D.B. Veprintsev, S. Grzesiek, Backbone NMR reveals allosteric signal transduction networks in the β_1-adrenergic receptor, Nature 530 (2016) 237–241.
[33] M. Casiraghi, M. Damian, E. Lescop, E. Point, K. Moncoq, N. Morellet, D. Levy, J. Marie, E. Guittet, J.L. Banères, L.J. Catoire, Functional modulation of a G protein-coupled receptor conformational landscape in a lipid bilayer, J. Am. Chem. Soc. 138 (2016) 11170–11175.
[34] F. Bumbak, A.C. Keen, N.J. Gunn, P.R. Gooley, R.A.D. Bathgate, D.J. Scott, Optimization and $^{13}CH_3$ methionine labeling of a signaling competent neurotensin receptor 1 variant for NMR studies, Biochim. Biophys. Acta Biomembr. 1860 (2018) 1372–1383.
[35] Y. Shiraishi, M. Natsume, Y. Kofuku, S. Imai, K. Nakata, T. Mizukoshi, T. Ueda, H. Iwaï, I. Shimada, Phosphorylation-induced conformation of β_2-adrenoceptor related to arrestin recruitment revealed by NMR, Nat. Commun. 9 (2018) 194.
[36] B. Franke, C. Opitz, S. Isogai, A. Grahl, L. Delgado, A.D. Gossert, S. Grzesiek, Production of isotope-labeled proteins in insect cells for NMR, J. Biomol. NMR 71 (2018) 173–184.
[37] M.T. Eddy, M.Y. Lee, Z.G. Gao, K.L. White, T. Didenko, R. Horst, M. Audet, P. Stanczak, K.M. McClary, G.W. Han, K.A. Jacobson, R.C. Stevens, K. Wüthrich, Allosteric coupling of drug binding and intracellular signaling in the A_{2A} adenosine receptor, Cell 172 (2018) 68–80.e12.
[38] L.D. Clark, I. Dikiy, K. Chapman, K.E. Rödström, J. Aramini, M.V. LeVine, G. Khelashvili, S.G. Rasmussen, K.H. Gardner, D.M. Rosenbaum, Ligand modulation of sidechain dynamics in a wild-type human GPCR, Elife 6 (2017).
[39] S. Reckel, D. Gottstein, J. Stehle, F. Löhr, M.K. Verhoefen, M. Takeda, R. Silvers, M. Kainosho, C. Glaubitz, J. Wachtveitl, F. Bernhard, H. Schwalbe, P. Güntert, V. Dötsch, Solution NMR structure of proteorhodopsin, Angew. Chem. Int. Ed. Eng. 50 (2011) 11942–11946.
[40] A. Gautier, H.R. Mott, M.J. Bostock, J.P. Kirkpatrick, D. Nietlispach, Structure determination of the seven-helix transmembrane receptor sensory rhodopsin II by solution NMR spectroscopy, Nat. Struct. Mol. Biol. 17 (2010) 768–774.
[41] L. Kooijman, P. Ansorge, M. Schuster, C. Baumann, F. Löhr, S. Jurt, P. Güntert, O. Zerbe, Backbone and methyl assignment of bacteriorhodopsin incorporated into nanodiscs, J. Biomol. NMR 74 (2020) 45–60.
[42] L. Ye, C. Neale, A. Sljoka, B. Lyda, D. Pichugin, N. Tsuchimura, S.T. Larda, R. Pomès, A.E. García, O.P. Ernst, R.K. Sunahara, R.S. Prosser, Mechanistic insights into allosteric regulation of the A_{2A} adenosine G protein-coupled receptor by physiological cations, Nat. Commun. 9 (2018) 1372.
[43] M.T. Eddy, Z.G. Gao, P. Mannes, N. Patel, K.A. Jacobson, V. Katritch, R.C. Stevens, K. Wüthrich, Extrinsic tryptophans as NMR probes of allosteric coupling in membrane proteins: application to the A_{2A} adenosine receptor, J. Am. Chem. Soc. 140 (2018) 8228–8235.
[44] C. Opitz, S. Isogai, S. Grzesiek, An economic approach to efficient isotope labeling in insect cells using homemade ^{15}N-, ^{13}C- and ^{2}H-labeled yeast extracts, J. Biomol. NMR 62 (2015) 373–385.
[45] L. Sušac, M.T. Eddy, T. Didenko, R.C. Stevens, K. Wüthrich, A_{2A} adenosine receptor functional states characterized by ^{19}F-NMR, Proc. Natl. Acad. Sci. U. S. A. 115 (2018) 12733–12738.
[46] T. Mizumura, K. Kondo, M. Kurita, Y. Kofuku, M. Natsume, S. Imai, Y. Shiraishi, T. Ueda, I. Shimada, Activation of adenosine A_{2A} receptor by lipids from docosahexaenoic acid revealed by NMR, Sci. Adv. 6 (2020) eaay8544.
[47] L.A. Abiko, A. Grahl, S. Grzesiek, High pressure shifts the β_1-adrenergic receptor to the active conformation in the absence of G protein, J. Am. Chem. Soc. 141 (2019) 16663–16670.
[48] J.N. Frei, R.W. Broadhurst, M.J. Bostock, A. Solt, A.J.Y. Jones, F. Gabriel, A. Tandale, B. Shrestha, D. Nietlispach, Conformational plasticity of ligand-bound and ternary GPCR complexes studied by ^{19}F NMR of the β_1-adrenergic receptor, Nat. Commun. 11 (2020) 669.
[49] M.P. Bokoch, Y. Zou, S.G. Rasmussen, C.W. Liu, R. Nygaard, D.M. Rosenbaum, J.J. Fung, H.J. Choi, F.S. Thian, T.S. Kobilka, J.D. Puglisi, W.I. Weis, L. Pardo, R.S. Prosser, L. Mueller, B.K. Kobilka, Ligand-specific regulation of the extracellular surface of a G-protein-coupled receptor, Nature 463 (2010) 108–112.
[50] R. Horst, J.J. Liu, R.C. Stevens, K. Wüthrich, β_2-adrenergic receptor activation by agonists studied with ^{19}F NMR spectroscopy, Angew. Chem. Int. Ed. Eng. 52 (2013) 10762–10765.
[51] A. Manglik, T.H. Kim, M. Masureel, C. Altenbach, Z. Yang, D. Hilger, M.T. Lerch, T.S. Kobilka, F.S. Thian, W.L. Hubbell, R.S. Prosser, B.K. Kobilka, Structural insights into the dynamic process of β_2-adrenergic receptor signaling, Cell 161 (2015) 1101–1111.
[52] T.H. Kim, K.Y. Chung, A. Manglik, A.L. Hansen, R.O. Dror, T.J. Mildorf, D.E. Shaw, B.K. Kobilka, R.S. Prosser, The role of ligands on the equilibria between functional states of a G protein-coupled receptor, J. Am. Chem. Soc. 135 (2013) 9465–9474.
[53] S. Imai, T. Yokomizo, Y. Kofuku, Y. Shiraishi, T. Ueda, I. Shimada, Structural equilibrium underlying ligand-dependent activation of β_2-adrenoreceptor, Nat. Chem. Biol. 16 (2020) 430–439.
[54] T. Ueda, Y. Kofuku, J. Okude, S. Imai, Y. Shiraishi, I. Shimada, Function-related conformational dynamics of G protein-coupled receptors revealed by NMR, Biophys. Rev. 11 (2019) 409–418.
[55] E. Trinquet, M. Fink, H. Bazin, F. Grillet, F. Maurin, E. Bourrier, H. Ansanay, C. Leroy, A. Michaud, T. Durroux, D. Maurel, F. Malhaire, C. Goudet, J.P. Pin, M. Naval, O. Hernout, F. Chrétien, Y. Chapleur, G. Mathis, D-myo-inositol 1-phosphate as a surrogate of D-myo-inositol 1,4,5-tris phosphate to monitor G protein-coupled receptor activation, Anal. Biochem. 358 (2006) 126–135.
[56] V. Tugarinov, L.E. Kay, Ile, Leu, and Val methyl assignments of the 723-residue malate synthase G using a new labeling strategy and novel NMR methods, J. Am. Chem. Soc. 125 (2003) 13868–13878.
[57] R. Kerfah, O. Hamelin, J. Boisbouvier, D. Marion, CH_3-specific NMR assignment of alanine, isoleucine, leucine and valine methyl groups in high molecular weight proteins using a single sample, J. Biomol. NMR 63 (2015) 389–402.
[58] S. Schütz, R. Sprangers, Methyl TROSY spectroscopy: a versatile NMR approach to study challenging biological systems, Progr. NMR Spectr. 116 (2020) 56–84.
[59] V. Tugarinov, R. Sprangers, L.E. Kay, Probing side-chain dynamics in the proteasome by relaxation violated coherence transfer NMR spectroscopy, J. Am. Chem. Soc. 129 (2007) 1743–1750.